

## Article

# Modeling CO<sub>2</sub>, H<sub>2</sub>S, COS, and CH<sub>3</sub>SH Simultaneous Removal Using Aqueous Sulfolane–MDEA Solution

Ke Liu <sup>1,2</sup>, Honggang Chang <sup>1,2</sup>, Gang Xiong <sup>1</sup>, Jinlong He <sup>1,2</sup>, Qisong Liu <sup>1,2</sup> and Jinjin Li <sup>1,2,\*</sup>

<sup>1</sup> Research Institute of Natural Gas Technology, PetroChina Southwest Oil & Gasfield Company, Chengdu 610213, China; diablo1klk@163.com (K.L.); changhg@petrochina.com.cn (H.C.); xiongg@petrochina.com.cn (G.X.); hejl@petrochina.com.cn (J.H.); qs\_liu@petrochina.com.cn (Q.L.)

<sup>2</sup> National Energy R&D Center of High-Sulfur Gas Exploitation, Chengdu 610213, China

\* Correspondence: lijijin621@163.com; Tel.: +86-135-6887-7658

**Abstract:** In this study, a rate-based absorption model coupled with an improved thermodynamic model was developed to characterize the removal of acid components (CO<sub>2</sub> and H<sub>2</sub>S) and organic sulfur (COS and CH<sub>3</sub>SH) from natural gas with an aqueous sulfolane–MDEA solution. First, the accuracy of the thermodynamic model was validated by comparing the calculated partial pressure of CO<sub>2</sub>, H<sub>2</sub>S, and CH<sub>3</sub>SH with those of the experimental data reported in the literature. Then, the industrial test data were employed to validate the absorption model and the simulation results agreed well with the experimental data. The average relative errors of the removal rates of CO<sub>2</sub>, COS, and CH<sub>3</sub>SH are 3.3%, 3.0%, 4.1%, respectively. Based on the validated coupled model, the total mass transfer coefficient and mass transfer resistance of each solute component at different column positions were analyzed. The effects of the gas–liquid ratio, overflow weir height, and absorption pressure on the absorption performance of each component were studied, and the influence of the acid component concentration in the feed gas on the removal efficiency of methyl mercaptan (CH<sub>3</sub>SH) was also discussed. It is found that the improved absorption model can better characterize the absorption performance and be conducive to the optimal design of the absorber column.

**Keywords:** absorption model; rate-based; organic sulfur; mass transfer



**Citation:** Liu, K.; Chang, H.; Xiong, G.; He, J.; Liu, Q.; Li, J. Modeling CO<sub>2</sub>, H<sub>2</sub>S, COS, and CH<sub>3</sub>SH Simultaneous Removal Using Aqueous Sulfolane–MDEA Solution. *Processes* **2021**, *9*, 1954. <https://doi.org/10.3390/pr9111954>

Academic Editor: Lin He

Received: 20 October 2021

Accepted: 29 October 2021

Published: 31 October 2021

**Publisher's Note:** MDPI stays neutral with regard to jurisdictional claims in published maps and institutional affiliations.



**Copyright:** © 2021 by the authors. Licensee MDPI, Basel, Switzerland. This article is an open access article distributed under the terms and conditions of the Creative Commons Attribution (CC BY) license (<https://creativecommons.org/licenses/by/4.0/>).

## 1. Introduction

With the development of society, natural gas is increasingly used in industry and daily life due to its economic and environmental advantages [1–3]. Since mined natural gas contains acid components (CO<sub>2</sub> and H<sub>2</sub>S) and organic sulfur (COS and CH<sub>3</sub>SH), it needs further treatment before it can be used [4–7]. Conventional gas processing includes distillation, adsorption, membrane separation, and absorption [8]. Among these purification techniques, chemical absorption is the most commonly used method for acid-gas removal in the natural gas industries with its high efficiency and simultaneous strip of multiple acid gases [9].

In the industry, aqueous amine solutions are often used to remove acid components from natural gas [10–12]. To overcome the limited capacity of organic sulfur components with amine solution, a mixed solvent containing sulfone is used because of the high gas loading for simultaneous absorption of high CO<sub>2</sub> and H<sub>2</sub>S content in raw gas. A common sulfone–amine solution is composed of N-methyl diethanolamine (MDEA), sulfolane, and water, which has an advantage in treating natural gas with high organic sulfur content [8,13]. Macgregor and Mather [14] reported the absorption of H<sub>2</sub>S and CO<sub>2</sub> with a mixed solvent consisting of MDEA (20.9 wt.%) + sulfolane (30.5 wt.%). Jou et al. [15] investigated acid-gas absorption with MDEA, methanethiol, and ethanethiol at 40 and 70 °C at thiol partial pressure within 0.1–15.8 kPa. Haghtalab et al. [16] measured the absorption of acid-gas in different mix solvents at 343 K and a total pressure of 0.1–0.21 kPa and reported variation in the solubility of CO<sub>2</sub> and H<sub>2</sub>S in different operating conditions and solvent compositions.

However, although absorption with various mixed solvents has been reported, reliable thermodynamic modeling of the absorption process remains a big challenge for simulating and optimization of the acid-gas capture processes [17].

In order to accurately simulate and design the absorption process of the acid component and organic sulfur in natural gas using an aqueous sulfolane–MDEA solution, it is necessary to establish a reliable and robust absorption model, which involves the gas–liquid equilibrium, chemical reaction equilibrium, material and heat balance, and transfer properties of each component in the system [18–20]. Afkhamipour and Mofarahi [21] compared the rate-based and equilibrium-stage models by simulating post-combustion CO<sub>2</sub> capture using a 2-amino-2-methyl-1-propanol (AMP) solution in a packed column. The simulation results of the absorber show that the rate-based model can better predict temperature and concentration curves than the equilibrium phase model. Al-Baghli et al. [22] simulated the process of removing CO<sub>2</sub> and H<sub>2</sub>S by MEA and DEA aqueous solutions using rate-based gas absorber model and obtained reliable simulation results. Pacheco and Rochelle [23] developed a framework to perform selective absorption of H<sub>2</sub>S using MDEA solution from a gas stream containing CO<sub>2</sub>. The Maxwell–Stefan and enhancement factor theories are used in the model. Mandal and Bandyopadhyay [24] conducted theoretical and experimental research on the simultaneous absorption of CO<sub>2</sub> and H<sub>2</sub>S into solutions containing MDEA and DEA. Moiola et al. [25] used the Eddy diffusivity theory in Aspen Plus and used an external subroutine to simulate the absorption of CO<sub>2</sub> and H<sub>2</sub>S from gas streams. In addition, they modified the parameters for vapor–liquid equilibrium (VLE) calculations and verified the simulation using data in the literature. Yang et al. [26] used an aqueous sulfone–MDEA solution to remove organic sulfur in natural gas and studied the factors that affect organic sulfur removal in natural gas purification devices. However, the process of the simultaneous removal of multiple impurities (i.e., CO<sub>2</sub>, H<sub>2</sub>S, COS, and CH<sub>3</sub>SH) is usually very complicated, and the influence of acidic gas on the absorption performance of organic sulfur during the removal process is still unclear.

In this study, we developed a rate-based absorption model coupled with an improved thermodynamic model to characterize the removal of acid components (CO<sub>2</sub> and H<sub>2</sub>S) and organic sulfur (COS and CH<sub>3</sub>SH) from natural gas with an aqueous sulfolane–MDEA solution. An improved thermodynamic model was used considering the influence of acid component concentration on the removal efficiency of methyl mercaptan (CH<sub>3</sub>SH). The mass transfer characteristics at different column positions were analyzed. The influence of the gas–liquid ratio, overflow weir height, and absorption pressure on the removal rate of each component and the influence of acid component content on the removal rate of methyl mercaptan (CH<sub>3</sub>SH) were studied. Furthermore, with the modified rate-based absorption model, we successfully simulated the adsorption process for a wide range of feed gas compositions and operating conditions. This study is expected to further facilitate optimization of the operating conditions and device structure.

## 2. Model Theory

### 2.1. Thermodynamic Framework

The detailed thermodynamic model consists of the gas–liquid equilibrium and chemical reaction equilibrium of each component in the solvent.

#### 2.1.1. Gas–Liquid Equilibrium

The gas–liquid equilibrium of the acid component (CO<sub>2</sub> and H<sub>2</sub>S) and organic sulfur (COS and CH<sub>3</sub>SH) in the aqueous sulfolane–MDEA solution is calculated by Henry’s law:

$$Py_i\varphi_i = H_i x_i \gamma_i^* \quad (1)$$

where  $P$  is the system pressure, Pa.  $H_i$  is Henry’s law constant of component  $i$  in the mixed solvent of water, sulfolane, and MDEA, Pa.  $y_i$  is the mole fraction of component  $i$  in the vapor phase, and  $x_i$  is the equilibrium mole fraction of component  $i$  in the liquid phase.  $\varphi_i$  is the fugacity coefficient of component  $i$  in the vapor phase, which is calculated using the

Peng–Robinson equation of state (EOS) [27].  $\gamma_i^*$  is the unsymmetric activity coefficient of component  $i$  in the mixed solvent solution of water, sulfolane, and MDEA.  $\gamma_i^*$  is normalized to the mixed solvent infinite dilution reference state.

In the mixed solvent, Henry's law constant can be calculated from those in the pure solvents, as shown in Equation (2) [28].

$$\ln\left(\frac{H_i}{\gamma_i^*}\right) = \sum_A w_A \cdot \ln\left(\frac{H_{iA}}{\gamma_{iA}^\infty}\right) \quad (2)$$

where  $\omega_A$  is the weighting factor, which can be calculated according to the method in the literature [13].  $\gamma_{iA}^\infty$  is the infinite dilution activity coefficient of component  $i$  in pure solvent A,  $H_{iA}$  is Henry's constant of component  $i$  in pure solvent A, and the values of  $H_{iA}$  of solute  $i$  (CO<sub>2</sub>, H<sub>2</sub>S and CH<sub>4</sub>) can be obtained directly from the literature [10–13]. Some  $H_{iA}$  values of CH<sub>4</sub>, CH<sub>3</sub>SH, and COS regressed according to the experimental data [29–31], which are summarized in Table 1.

**Table 1.** Parameters for Henry's constant.

Solute $i$	Solvent A	A	B	C	D	Data Source
CH <sub>4</sub>	sulfolane	26.68	−1538.38	0	0.02	Jou et al. [31]
CH <sub>3</sub> SH	H <sub>2</sub> O	21.128	−1299.310	0	0	Bedell and Miller [29]
CH <sub>3</sub> SH	sulfolane	12.987	0	0	0	Bedell and Miller [29]
COS	H <sub>2</sub> O	27.402	−2407.192	0	0	Al-Ghawas et al. [32]
COS	MDEA	19.323	−603.363	0	0	Al-Ghawas et al. [32]
COS	sulfolane	11.004	0.170	0	0.015	Shokouhi et al. [30]

During the absorption process, MDEA reacted with acidic components and the amount of reaction affected the absorption of organic sulfur in the aqueous sulfolane–MDEA solution. Thus, the unreacted ratio of MDEA is introduced to modify Henry's coefficient of methyl mercaptan (CH<sub>3</sub>SH) in the aqueous sulfolane–MDEA solution [26]. Equation (3) is used to quantitatively describe the influence of the acid component content on Henry's constant for CH<sub>3</sub>SH.

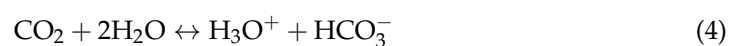
$$H_{CH_3SH} = \frac{H'_{CH_3SH}}{f^C} \quad (3)$$

where  $f$  is the unreacted ratio of MDEA, which is the ratio between unreacted MDEA and the total amount of MDEA and MDEAH<sup>+</sup> in aqueous solutions.  $C$  is the effect factor, symbolizing the influence of the acid component on Henry's law constant.  $H'_{CH_3SH}$  and  $H_{CH_3SH}$  are Henry's constants of CH<sub>3</sub>SH in the mixed solvent when the influence of acid component is not taken into account and is taken into consideration, respectively.

The electrolyte-nonrandom two-liquid (e-NRTL) model is used to calculate the activity coefficients [33]. The molecule–molecule, electrolyte–electrolyte, and molecule–electrolyte binary parameters are mainly obtained from the literature [10,13]. Some binary parameters that are not mentioned in the literature are defaulted to (8, −4), and the non-randomness factor is fixed at 0.2 [34].

### 2.1.2. Aqueous Phase Chemical Equilibrium

In aqueous solutions, the acid components H<sub>2</sub>S and CO<sub>2</sub> react with MDEA, and the ionic equilibrium reactions are expressed as Equations (4)–(9) [35].





The liquid phase compositions must satisfy the chemical equilibrium relationships [11]:

$$K_j = \frac{\prod_{i'} (x_{i'} \gamma_{i'})^{v_{i'}}}{\prod_i (x_i \gamma_i)^{v_i}} \quad (10)$$

where  $K_j$  is the chemical equilibrium constant of reaction  $j$ ,  $x_i$  is the mole fraction of reactant component  $i$  in reaction  $j$ ,  $x_{i'}$  is the mole fraction of product component  $i'$  in reaction  $j$ , and  $\gamma_i$  and  $\gamma_{i'}$  are the unsymmetric activity coefficients of reactant component  $i$  and product component  $i'$  in the aqueous solution. The unsymmetric activity coefficients are normalized to the aqueous phase infinite dilution reference state.  $v_i$  and  $v_{i'}$  represent the stoichiometric coefficients of reactants and products, respectively.

The chemical equilibrium constant  $K_j$  of reaction  $j$  can be calculated by Equation (11) [11,35].

$$\ln(K_j) = A + \frac{B}{T} + C \ln(T) + DT \quad (11)$$

where the constants  $A$ ,  $B$ ,  $C$  and  $D$  are summarized in Table 2.

**Table 2.** Parameters for temperature-dependent mole-fraction reaction equilibrium constants.

Reaction	A	B/T	C	D/K <sup>-1</sup>	T Range/K	Source
4	819.8	−37655.9	−124.5	0	273–498	In this Work <sup>a</sup>
5	−553.4	28412.7	77.7	0	273–423	In this Work <sup>a</sup>
6	−9.4165	−4234.98	0	0	298–333	Austgen et al. [36]
7	−32.0	−3338.0	0	0	287–343	Austgen et al. [36]
8	216.049	−12431.7	−35.4819	0	273–498	Austgen et al. [36]
9	132.899	−13445.9	−22.4773	0	273–498	Austgen et al. [36]

<sup>a</sup> The equilibrium reaction order of CO<sub>2</sub> and H<sub>2</sub>S are obtained by fitting the experimental data. The reaction orders of CO<sub>2</sub> and HCO<sub>3</sub><sup>−</sup> are 1.25, the reaction orders of H<sub>2</sub>S and HS<sup>−</sup> are 1.35, and the reaction orders of the remaining reactions are 1.

## 2.2. Rate-Based Model Assumptions

In order to simulate the absorption process of removing the acid component (H<sub>2</sub>S and CO<sub>2</sub>) and organic sulfur (COS and CH<sub>3</sub>SH) from natural gas utilizing a tray column, a mathematical model was established using the two-film theory [37]. The basic assumptions are as follows:

- (1) Consider both physical absorption and chemical absorption, and the reaction only occurs in the liquid phase.
- (2) The absorption column is adiabatic.
- (3) The heat transfer resistance of the liquid phase is neglected, and the interface temperature is equal to the bulk temperature.
- (4) Flow is one-dimensional in the axial direction, and the radial temperature and concentration variation can be neglected.

## 2.3. Material and Energy Balance

The tray column is composed of many stages, where vapor and liquid streams from adjacent stages contact each other and exchange mass and energy at their common interface [18,21].

Figure 1. Presents a stage  $j$  in the tray column, and  $i$  represents the components. The main mass and energy balance equations are listed below [38].

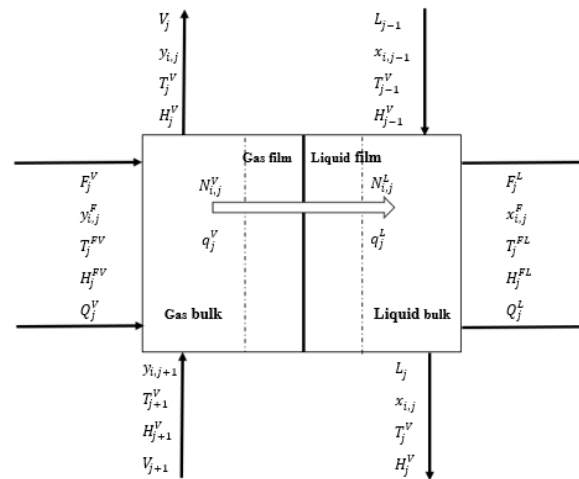


Figure 1. Rate-based stage model.

Material balance for liquid phase:

$$F_j^L x_{i,j}^F + L_{j-1} x_{i,j-1} + N_{i,j}^L + r_{i,j}^L - L_j x_{i,j} = 0 \quad (12)$$

Material balance for vapor phase:

$$F_j^V y_{i,j}^F + V_{j+1} y_{i,j-1} + N_{i,j}^V - V_j y_{i,j} = 0 \quad (13)$$

Energy balance for liquid phase:

$$F_j^L H_j^{FL} + L_{j-1} H_{j-1}^L + Q_j^L + q_j^L - L_j H_j^L = 0 \quad (14)$$

Energy balance for vapor phase:

$$F_j^V H_j^{FV} + V_{j+1} H_{j-1}^V + Q_j^V + q_j^V - V_j H_j^V = 0 \quad (15)$$

where  $F$  is the mole flow rate of feed,  $\text{kmol s}^{-1}$ .  $L$  and  $V$  represent the mole flow rates of liquid and vapor, respectively,  $\text{kmol s}^{-1}$ .  $N$  is the mole transfer rate,  $\text{kmol s}^{-1}$ .  $r$  is the reaction rate, which can be calculated from the component concentration.  $x_i$  and  $y_i$  are the mole fractions of component  $i$  in the liquid and vapor phases, respectively.  $Q$  is the heat input to a stage,  $\text{J s}^{-1}$ ;  $q$  is the heat transfer rate,  $\text{J s}^{-1}$ ;  $H^{FL}$  and  $H^{FV}$  are the enthalpies of the inflow liquid and inflow vapor,  $\text{J kmol}^{-1}$ ; and the thermodynamic properties including enthalpy and heat capacity utilized in heat transfer calculations can be obtained directly from the literature [10–13].

#### 2.4. Mass Transfer and Enhancement Factor

The mass transfer flux between the gas phase and the liquid phase is shown in Equation (16) [39].

$$N_i = K_{G,i} (P_i - P_i^*) a_p A_c \quad (16)$$

where  $K_{G,i}$  is the overall mass transfer coefficient for component  $i$ ;  $a_p$  is the effective mass transfer area per unit area of the tray,  $\text{m}^2 \text{m}^{-2}$ ;  $A_c$  is the cross-sectional area of the column,  $\text{m}^2$ ;  $P_i$  is the partial pressure of component  $i$  in the gas bulk; and  $P_i^*$  is the partial pressure of component  $i$  in equilibrium with the liquid phase. The partial pressure of each component can be calculated by the established thermodynamic model.

Using the two-film model, the overall mass transfer coefficients incorporating gas and liquid transfer resistance for component  $i$  is expressed as Equation (17).

$$\frac{1}{K_{G,i}} = \frac{1}{k_{G,i}} + \frac{H_i}{k_{L,i} E_i} \quad (17)$$

Where  $H_i$  is Henry's law constant of component  $i$ ;  $K_{G,i}$  is the overall mass transfer of component  $i$  in gas phase; and  $k_{G,i}$  and  $k_{L,i}$  are the mass transfer coefficient of component  $i$  without reaction in the gas phase and the liquid phase, which are calculated according to the method used by Simon et al. [18] and Saimpert et al. [40]. The density, viscosity, and surface tension required for the calculation can be obtained directly from the Aspen database.  $E_i$  is the enhancement factor of component  $i$  due to chemical reactions, which is the ratio of the mass transfer enhanced by a reaction over the mass transfer without the reaction [21]. The calculation of the enhancement factor in this work uses the formula developed by Danckwerts [41].

For large values of enhancement factor for infinite fast reaction ( $E_\infty$ ) and Hatta numbers lower than 2, the enhancement factor is calculated using a simplified Equation (18) [42].

$$E_i = \frac{Ha}{\tanh(Ha)} \quad (18)$$

For infinite fast reaction ( $E_\infty$ ) values lower than 100 and Hatta numbers larger than 2, the enhancement factor is calculated using a simplified Equation (19) [1].

$$E_i = \left( \frac{E_\infty - 1}{Ha^{3/2}} + \frac{1}{E_\infty^{3/2}} \right)^{-2/3} \quad (19)$$

where the Hatta number and enhancement factor for the infinite fast reaction are expressed as Equations (20) and (21) [42].

$$Ha = \frac{\sqrt{k_{2t,i} \cdot D_{i,L} \cdot C_{MDEA}^{Bulk}}}{k_{L,i}} \quad (20)$$

$$E_\infty = 1 + \frac{D_{MDEA,L}}{D_{i,L}} \times \frac{C_{MDEA}^{Bulk}}{C_i^{In}} \quad (21)$$

where  $D_{i,L}$  refers to the diffusivity of absorption component  $i$  in an aqueous sulfolane-MDEA solution,  $D_{MDEA,L}$  is the diffusivity of the MDEA in the liquid phase.  $C_i^{In}$  is the concentration of absorption component  $i$  at the gas-liquid interface, and  $C_{MDEA}^{Bulk}$  represents the concentration of MDEA in the bulk liquid. Pacheco and Rochelle [23] and Al-Ghawas et al. [32] measured the rate constants of reaction between  $CO_2$  and MDEA and between COS and MDEA in the mixed solvent, respectively, as shown in Equations (22) and (23).

$$k_{2t,CO_2} = 2.576 \times 10^9 \exp(-6024/T) \quad (22)$$

$$k_{2t,COS} = 4198.74 \exp(-4575.80/T) \quad (23)$$

For  $CO_2$  and COS, the enhancement factor is needed for the mass transfer rate calculations, which are calculated using Equation (18). As the reaction between  $H_2S$  and MDEA is very fast, the enhancement factor can be calculated using the infinite fast reaction rate, as shown in Equation (19). In contrast, the absorption of  $CH_3SH$  is mainly a physical effect, so there is also no need to consider the influence of chemical reactions.

### 2.5. Computational Implementation

The model calculation was performed by writing Fortran programs. The solution of the absorption model adopts the stepwise calculation method, and the steps are as follows:

(1) The concentration of the absorbed components in the gas and liquid feed, and the gas-liquid ratio are known. By assuming the total removal rate of each component, the concentration of each absorbed component in the liquid at the last plate can be calculated.

(2) Since the concentration of gas feed and liquid discharge of the last plate is known, the concentration of liquid feed and gas discharge of this plate, that is, the concentration of gas feed and liquid discharge of the upper plate can be calculated.

(3) It is calculated upward until the gas discharge concentration of the top plate is obtained, then the removal rate of the whole column of each component can be calculated.

(4) Compare the removal rate of the whole tower between the hypothesis and the calculated one. If the error is greater than 0.0001, change the hypothesis and continue the iterative calculation until the error requirement is met.

### 3. Modeling Results

As mentioned above, a rate-based absorption model coupled with the thermodynamic model was developed for the removal of acid components ( $\text{CO}_2$  and  $\text{H}_2\text{S}$ ) and organic sulfur ( $\text{COS}$  and  $\text{CH}_3\text{SH}$ ) from natural gas with an aqueous sulfolane–MDEA solution.

In this section, the accuracies of the thermodynamic model and absorption model are first validated. Then, the effects of the gas–liquid ratio, overflow weir height, and absorption pressure on the absorption performance of each component are investigated, and finally, the influence of acid component concentration in the feed gas on the removal efficiency of methyl mercaptan ( $\text{CH}_3\text{SH}$ ) is also discussed.

#### 3.1. Thermodynamics Model Validation

An improved thermodynamic model was employed to calculate the solubility and partial pressure of acid components and organic sulfur in the aqueous sulfone–MDEA solution. The experimental data of several systems are employed to verify the accuracy of the thermodynamic model.

Figures 2 and 3 display the experimental and calculated  $\text{CO}_2$  partial pressure data for the  $\text{CO}_2$ – $\text{H}_2\text{O}$ –MDEA system and  $\text{H}_2\text{S}$  partial pressure data for the  $\text{H}_2\text{S}$ – $\text{H}_2\text{O}$ –MDEA system at different compositions and different temperatures. As shown, the calculated  $\text{CO}_2$ / $\text{H}_2\text{S}$  partial pressure values are in good agreement with the experimental data reported by the literature [14,43–45], thus validating the proposed thermodynamic model. From Figure 2, it is found that the  $\text{CO}_2$  partial pressure is more sensitive to temperature. With the temperature increasing from 313.15 K to 338.75 K, the  $\text{CO}_2$  partial pressure experiences a significant increase. However, the MDEA mass fraction seems to have little effect on the  $\text{CO}_2$  partial pressure when the temperature is 313.15 K. Figure 3 shows the comparison of experimental data and calculated data in terms of  $\text{H}_2\text{S}$  partial pressure for the  $\text{H}_2\text{S}$ – $\text{H}_2\text{O}$ –MDEA system. As shown, the proposed thermodynamic model is also effective and robust. This means that the improved thermodynamic model has good applicability.

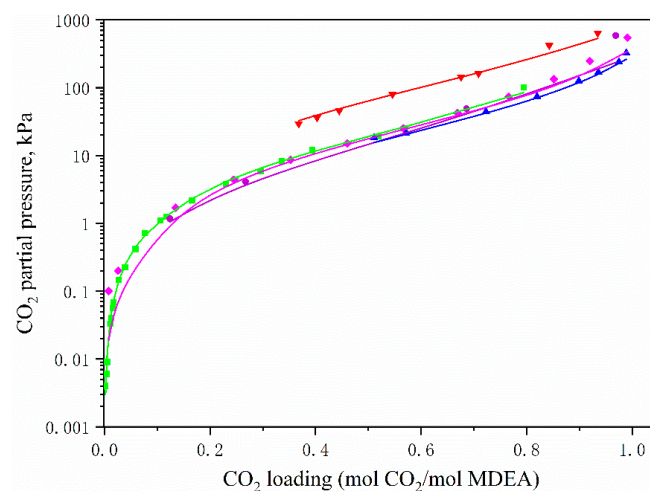


**Figure 2.** Comparison of experimental data and calculated data of the  $\text{CO}_2$ – $\text{H}_2\text{O}$ –MDEA system under different conditions. ■, measured by Jou et al. [43],  $T = 313.15$  K, MDEA mass fraction = 0.35; ●, measured by Macgregor and Mather [14],  $T = 313.15$  K, MDEA mass fraction = 0.209; ▲, measured by Qian et al. [44],  $T = 310.95$  K, MDEA mass fraction = 0.20; ▼, measured by Qian et al. [44],  $T = 338.75$  K, MDEA mass fraction = 0.20; and ◆, measured by Sidi-Boumedine et al. [45],  $T = 313.15$  K, MDEA mass fraction = 0.257. The solid line represents the calculated data in this work.

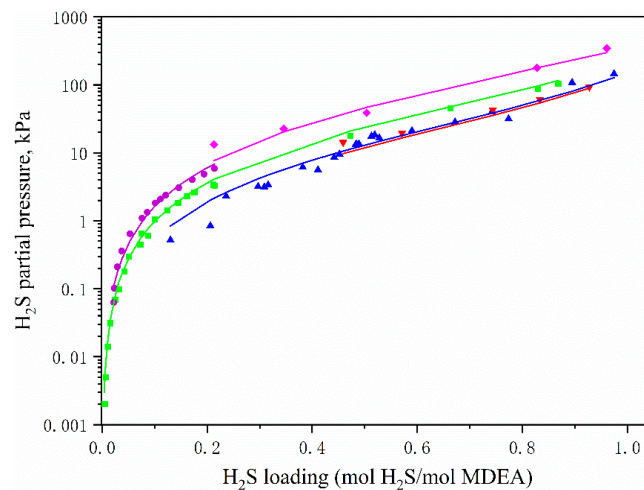


**Figure 3.** Comparison of experimental data and calculated data of the  $\text{H}_2\text{S}$ – $\text{H}_2\text{O}$ –MDEA system under different conditions.  $\blacksquare$ , measured by Jou et al. [43],  $T = 313.15$  K, MDEA mass fraction = 0.35;  $\bullet$ , measured by Jou et al. [43],  $T = 313.15$  K, MDEA mass fraction = 0.50;  $\blacktriangle$ , measured by Macgregor and Mather [14],  $T = 310.95$  K, MDEA mass fraction = 0.209;  $\blacktriangledown$ , measured by Qian et al. [44],  $T = 338.75$  K, MDEA mass fraction = 0.20; and  $\blacklozenge$ , measured by Qian et al. [44],  $T = 338.75$  K, MDEA mass fraction = 0.20. The solid line represents the calculated data in this work.

When compared with an aqueous amine solution, an aqueous sulfone–amine solution is more effective, especially for raw gas with high organic sulfur content. A common sulfone–amine solution is composed of MDEA, sulfolane, and water. Herein, two systems, namely the  $\text{CO}_2$ – $\text{H}_2\text{O}$ –sulfolane–MDEA system and the  $\text{H}_2\text{S}$ – $\text{H}_2\text{O}$ –sulfolane–MDEA system, are used to validate the thermodynamic model. The comparison results of the calculated values and experimental data in terms of  $\text{CO}_2/\text{H}_2\text{S}$  partial pressure are given in Figures 4 and 5. As shown, the calculated results agree well with the experimental data in terms of  $\text{CO}_2/\text{H}_2\text{S}$  partial pressure. Generally, the addition of sulfolane is beneficial to enhancing the absorption of acidic gases, and therefore, high acidic gas loading is observed at low partial pressure. When compared with Figures 4 and 5, it can be found that  $\text{H}_2\text{S}$  has a higher solubility than  $\text{CO}_2$  in the  $\text{H}_2\text{O}$ –sulfolane–MDEA solution.

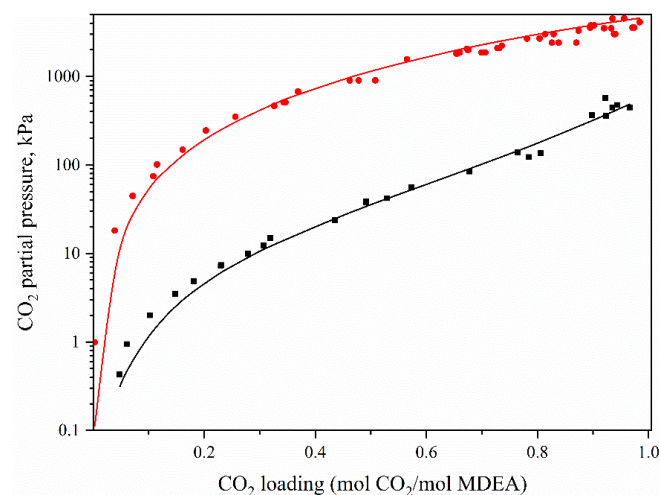


**Figure 4.** Comparison of the experimental data and calculated data for the  $\text{CO}_2$ – $\text{H}_2\text{O}$ –sulfolane–MDEA system under different conditions.  $\blacksquare$ , measured by Jou et al. [43],  $T = 313.15$  K, MDEA mass fraction = 0.305, sulfolane mass fraction = 0.209;  $\bullet$ , measured by Jou et al. [43],  $T = 373.15$  K, MDEA mass fraction = 0.305, sulfolane mass fraction = 0.209. The solid line represents the calculated data in this work.

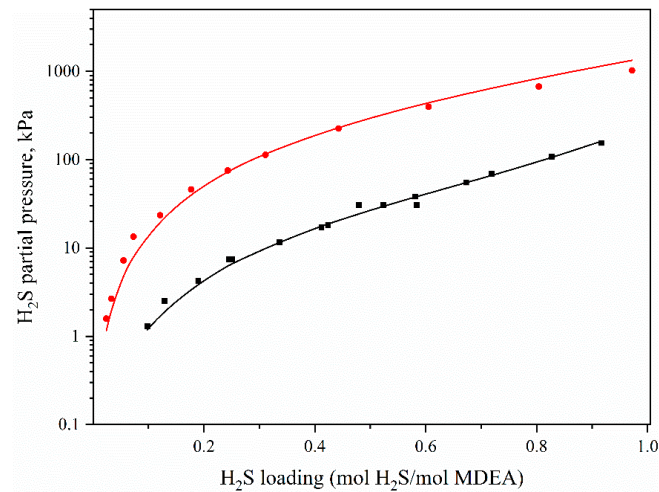


**Figure 5.** Comparison of the experimental data and calculated data of the H<sub>2</sub>S–H<sub>2</sub>O–sulfolane–MDEA system under different conditions. ■, measured by Jou et al. [43], T = 313.15 K, MDEA mass fraction = 0.305, sulfolane mass fraction = 0.209; ●, measured by Jou et al. [43], T = 373.15 K, MDEA mass fraction = 0.305, sulfolane mass fraction = 0.209. The solid line represents the calculated data in this work.

In order to further verify the reliability of the thermodynamic model, some CO<sub>2</sub> and H<sub>2</sub>S partial pressure data calculated in this paper are compared with the values calculated with reaction parameters proposed by Austgen et al. [36]. The average relative deviations of the partial pressure data of CO<sub>2</sub> and H<sub>2</sub>S calculated in this paper are 10.7% and 24.4%, respectively, while the average relative deviations of the partial pressure data calculated with reaction parameters proposed by Austgen et al. [36] are 38.1% and 36.8%, respectively. The calculated results using the improved thermodynamic model are not only in good agreement with the experimental data but also better than the calculated values of the existing models in the literature (see Figures 6 and 7). This is because we refitted the exponents of the equilibrium equations of reactions (4) and (5) and calculated the reaction equilibrium constants with the new parameters in Table 2.

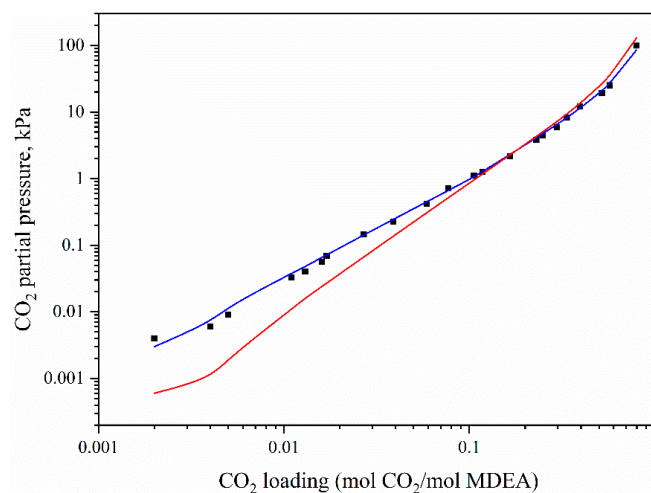


**Figure 6.** Comparison of the calculated data in the reference and in this work for the CO<sub>2</sub>–H<sub>2</sub>O–MDEA system. ■, experimental data measured by Jou et al. [43]; —, data calculated with the reaction parameters proposed by Austgen et al. [36]; —, data calculated in this work.

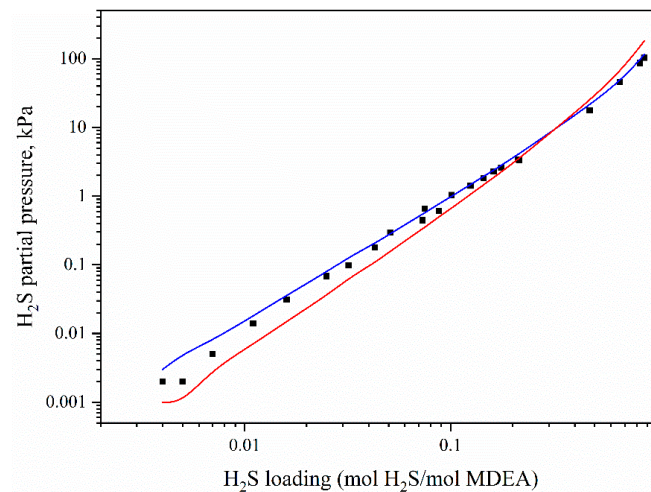


**Figure 7.** Comparison of the calculated data in the reference and in this work for the  $\text{H}_2\text{S}$ – $\text{H}_2\text{O}$ –MDEA system. ■, experimental data measured by Jou et al. [43]; —, data calculated with the reaction parameters proposed by Austgen et al. [36]; and —, data calculated in this work.

To verify the prediction performance of the improved thermodynamic model on the partial pressure data of  $\text{CH}_3\text{SH}$  in the system, the calculated value of the model is compared with the value measured by Jou et al. [15] in Figure 8. It can be seen that the predicted  $\text{CH}_3\text{SH}$  partial pressure data are in good agreement with the experimental value. This shows that the improved thermodynamic model not only has higher prediction accuracy but also has a larger application range.

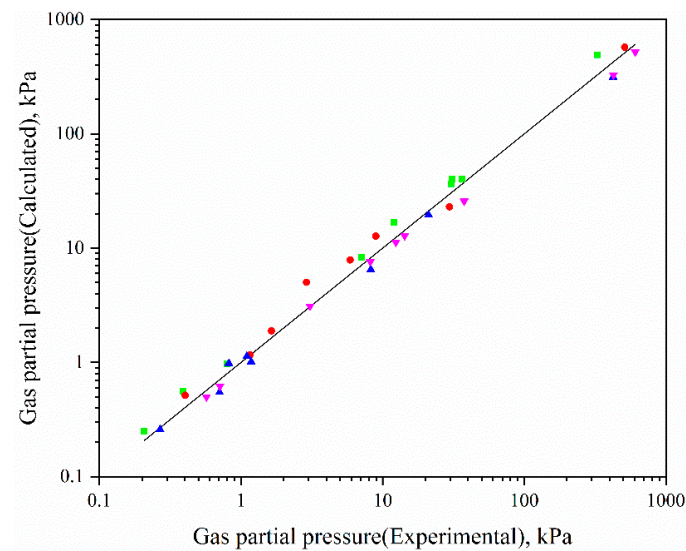


**Figure 8.** Parity plot for  $\text{CH}_3\text{SH}$  partial pressure, experimental data vs. model predictions.  $\text{CH}_3\text{SH}$ – $\text{H}_2\text{O}$ –MDEA system: ■,  $T = 313.15$  K, MDEA mass fraction = 0.50; ▲,  $T = 343.15$  K, MDEA mass fraction = 0.50.  $\text{CO}_2$ – $\text{H}_2\text{S}$ – $\text{CH}_3\text{SH}$ – $\text{H}_2\text{O}$ –MDEA system: ●,  $T = 313.15$  K, MDEA mass fraction = 0.50; ▼,  $T = 343.15$  K, MDEA mass fraction = 0.50.

In short, the proposed thermodynamic model has strong applicability, and its accuracy has been verified by various experimental data. In this study, the thermodynamic model is employed to calculate the solubility and partial pressure of acid components and organic sulfur in the aqueous sulfone–MDEA solution.

### 3.2. Rate-Based Absorption Model Validation

Before the rate-based model is applied to investigate the absorption process, its accuracy must be verified. The data were collected on an industrial sieve plate tower of 3.4 m in diameter with a mixed solvent comprising 20 wt% H<sub>2</sub>O, 40 wt% sulfolane, and 40 wt% MDEA. The tower was operated under a different number of plates (22, 26, and 30) and overflow weir heights (0.1 and 0.15 m). The Inlet gas–liquid ratio (vol./vol.) was adjusted from 490.2 to 720.0. CO<sub>2</sub> and H<sub>2</sub>S loading were varied from 4.11 vol% to 4.73 vol% and 1.34 vol% to 1.57 vol%, respectively. The concentration of CH<sub>3</sub>SH and COS were changed from 14.12 to 25.41 mg/m<sup>3</sup> and 11.18 to 34.58 mg/m<sup>3</sup>, respectively. As shown in Table 3, the simulation results of removal efficiency for absorption components are in good agreement with the data from the industrial absorber. For CO<sub>2</sub>, COS, and CH<sub>3</sub>SH, the average relative errors are only 3.3%, 3.0%, and 4.1%, respectively. Therefore, the rationality of the absorption model can be confirmed.

### 3.3. Rate-Based Absorption Model Calculation

The specifications and operating parameters of the absorption column are summarized in Table 4, and the mass fractions of H<sub>2</sub>O, sulfolane, and MDEA in the mixed solvent are 0.20, 0.40, and 0.40, respectively. The parameters of the absorber are obtained from (the desulfurizing column of) PetroChina Southwest Oil and Gasfield Company, and the operating parameters are obtained by analyzing the operating parameters of typical industrial absorbers and by making appropriate extensions.

The concentration profile of each component and the gas–liquid temperature profile are also obtained. As shown in Figure 9, the absorption rate of H<sub>2</sub>S is fast, and the concentration of H<sub>2</sub>S in the feed gas drops rapidly after entering the absorption column; it is completely removed in the middle of the column. This is the result of the synergistic effect of physical absorption and chemical reaction. However, the absorption rate of CH<sub>3</sub>SH is low. After the feed gas enters the column, the concentration of CH<sub>3</sub>SH decreases slowly and the final removal rate is low. The main reason for this is that the physical adsorption and absorption processes are controlled by equilibrium.

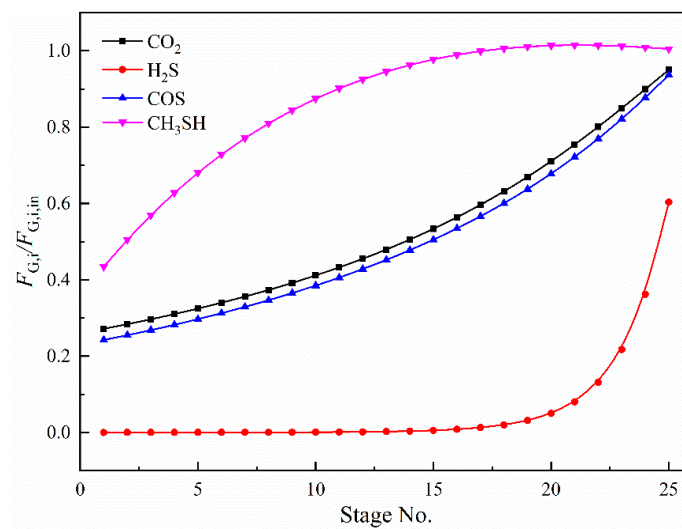


**Figure 9.** The concentration profile of each component in the absorption column (overflow weir height: 0.15 m; absorption pressure: 6 MPa; inlet gas flow rate:  $5.0 \times 10^6$  Nm<sup>3</sup>/d; inlet gas–liquid ratio: 600; inlet gas loading: CO<sub>2</sub>, 4.5 vol.%; H<sub>2</sub>S, 1.5 vol.%; COS, 15 mg/m<sup>3</sup>; and CH<sub>3</sub>SH, 15 mg/m<sup>3</sup>).

Table 3. Comparison of experiment data and model calculation data from the industry.

Experimental No.	Number of Plates	Overflow Weir Height (m)	Inlet Gas Flow Rate ( $10^4$ Nm <sup>3</sup> /d)	Inlet Gas-Liquid Ratio (vol/vol)	Pressure (Mpa)	Inlet Gas Loading H <sub>2</sub> S (vol.%)	Inlet Gas Loading CO <sub>2</sub> (vol.%)	CH <sub>3</sub> SH Concentration (mg/m <sup>3</sup> )	COS Concentration (mg/m <sup>3</sup> )	Experimental Removal Efficiency (%)			Simulated Removal Efficiency (%)		
										CO <sub>2</sub>	COS	CH <sub>3</sub> SH	CO <sub>2</sub>	COS	CH <sub>3</sub> SH
1	26	0.15	384.0	490.2	6.14	1.49	4.26	15.53	12.33	74.1	82.9	76.9	76.4	80.2	70.7
2	26	0.15	417.0	568.4	6.14	1.44	4.17	15.62	14.64	70.4	79.2	61.9	72.6	78.3	62.8
3	26	0.15	446.0	608.6	6.13	1.41	4.32	15.53	11.18	73.3	78.0	56.3	73.1	78.4	58.1
4	30	0.15	535.2	614.3	6.20	1.55	4.62	22.42	32.53	73.4	79.4	57.7	73.4	80.3	58.6
5	26	0.15	458.0	622.8	6.13	1.41	4.31	15.75	13.78	76.6	76.6	53.9	72.6	78.1	56.8
6	26	0.15	553.0	645.4	6.11	1.49	4.73	20.20	41.18	69.7	81.1	56.8	70.3	76.5	54.0
7	30	0.15	553.4	655.1	6.44	1.57	4.58	25.41	34.58	74.8	79.7	52.1	76.6	82.0	56.1
8	26	0.15	570.0	659.7	6.18	1.50	4.71	19.40	29.94	68.8	79.1	51.2	70.9	76.9	53.2
9	26	0.15	442.0	661.1	6.18	1.40	4.28	16.09	23.57	72.0	79.1	51.5	72.1	78.2	54.0
10	30	0.15	600.2	661.8	6.11	1.52	4.26	24.39	28.08	70.4	76.7	50.5	71.8	79.0	53.7
11	26	0.15	448.0	662.4	6.18	1.41	4.17	16.12	24.29	73.6	79.1	50.4	71.7	77.9	54.1
12	26	0.15	596.0	665.8	6.11	1.51	4.23	23.49	19.78	67.8	75.9	54.1	69.3	75.3	53.2
13	22	0.15	600.0	666.0	6.11	1.52	3.69	20.54	20.81	57.1	67.2	53.2	59.5	67.6	54.5
14	22	0.15	602.3	673.0	6.10	1.51	4.49	24.33	25.01	61.0	71.0	54.0	59.5	67.9	52.7
15	30	0.15	612.0	674.3	6.19	1.51	4.31	24.31	31.01	66.8	74.3	56.6	71.7	79.0	53.3
16	26	0.15	589.0	681.2	6.16	1.50	4.51	14.85	21.59	66.7	70.9	52.9	68.9	75.6	51.9
17	26	0.15	614.7	720.0	6.26	1.51	4.48	17.42	17.45	66.7	75.9	47.7	69.3	76.0	49.5
18	26	0.1	475.0	547.6	6.19	1.35	4.34	15.49	17.66	67.0	61.2	66.3	65.9	63.0	65.0
19	26	0.1	399.0	558.9	6.15	1.39	4.37	15.23	11.90	71.6	64.8	66.5	68.5	65.9	63.2
20	30	0.1	412.0	575.8	6.14	1.38	4.18	14.63	11.82	68.4	66.1	63.2	71.2	68.2	62.4
21	26	0.1	407.0	576.0	6.15	1.39	4.30	14.95	11.57	70.0	61.7	63.0	67.9	65.4	61.6
22	30	0.1	414.0	582.3	6.15	1.38	4.37	14.12	12.23	67.7	68.9	64.2	71.6	68.9	61.4
23	30	0.1	448.0	630.8	6.14	1.38	4.15	14.26	13.48	68.4	67.7	53.2	72.7	71.0	56.4
24	26	0.1	599.0	653.3	6.27	1.45	4.23	16.70	26.95	60.8	57.3	52.9	61.8	59.6	56.2
25	26	0.1	470.0	653.8	6.22	1.36	4.11	15.48	9.35	65.9	61.3	56.6	65.2	63.0	55.6
26	30	0.1	595.0	656.2	6.42	1.35	4.53	17.76	25.27	65.6	63.3	55.1	68.3	66.5	56.5
27	22	0.1	605.0	660.6	6.26	1.34	4.53	17.78	24.15	61.1	55.7	53.6	55.5	54.0	55.1
28	26	0.1	602.0	661.0	6.51	1.46	4.58	18.48	30.04	62.7	59.5	57.1	62.6	60.7	57.0
29	30	0.1	603.0	663.6	6.45	1.45	4.41	17.35	27.17	66.3	63.1	56.9	68.8	67.2	56.2
30	26	0.1	597.0	664.9	6.25	1.41	4.45	17.15	28.45	61.8	56.8	59.5	61.5	59.7	54.7
31	22	0.1	599.0	671.3	6.31	1.35	4.50	17.21	28.49	61.1	55.1	57.0	55.3	53.7	54.8
32	22	0.1	612.0	681.6	6.35	1.35	4.60	17.72	29.77	58.9	53.6	54.7	55.2	53.8	54.2

**Table 4.** Specifications of the absorber column and typical operating data.

Parameters	Data
Column diameter (m)	3.4
Number of plates	25
Overflow weir height (m)	0.08–0.2
Inlet gas flow rate ( $10^4 \text{ Nm}^3/\text{d}$ )	500
Inlet gas temperature ( $^{\circ}\text{C}$ )	40
Inlet liquid temperature ( $^{\circ}\text{C}$ )	20
Inlet gas-liquid ratio	400–800
Absorption pressure (MPa)	4.0–8.0
Inlet gas loading $\text{CO}_2$ (vol.%)	0–6.0
Inlet gas loading $\text{H}_2\text{S}$ (vol.%)	0–6.0
$\text{CH}_3\text{SH}$ concentration ( $\text{mg}/\text{m}^3$ )	15.0
$\text{COS}$ concentration ( $\text{mg}/\text{m}^3$ )	15.0

Physical absorption and chemical reactions are usually accompanied by a thermal effect, which changes the system temperature and, in turn, affects the absorption of components. Therefore, the temperature of the absorber column needs to be strictly controlled. Figure 10 shows the gas and liquid phase temperatures in the column at different concentrations of  $\text{H}_2\text{S}$  and  $\text{CO}_2$ . It can be seen that the gas phase and the liquid phase exchange heat in the column, and as the concentration of  $\text{H}_2\text{S}$  and  $\text{CO}_2$  increases, the heat release during the absorption process increases, resulting in an increase in the outlet temperature of the liquid phase at the top of the column. When the feed composition is the same, the  $\text{H}_2\text{S}$  is completely absorbed in the middle section of the column, and then the heat release is rapidly reduced, resulting in a rapid drop in the gas phase temperature at the top of the column.

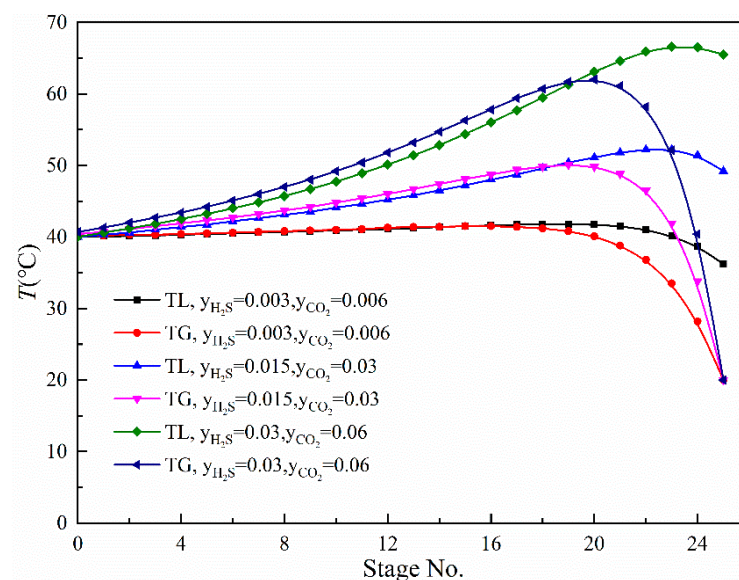


**Figure 10.** The gas–liquid temperature profile of each component in the absorption column (overflow weir height: 0.15 m; absorption pressure: 6 MPa; inlet gas flow rate:  $5.0 \times 10^6 \text{ Nm}^3/\text{d}$ ; inlet gas–liquid ratio: 600).

The calculated total mass transfer coefficient and mass transfer resistance of each solute component at different column positions are shown in Figure 11.

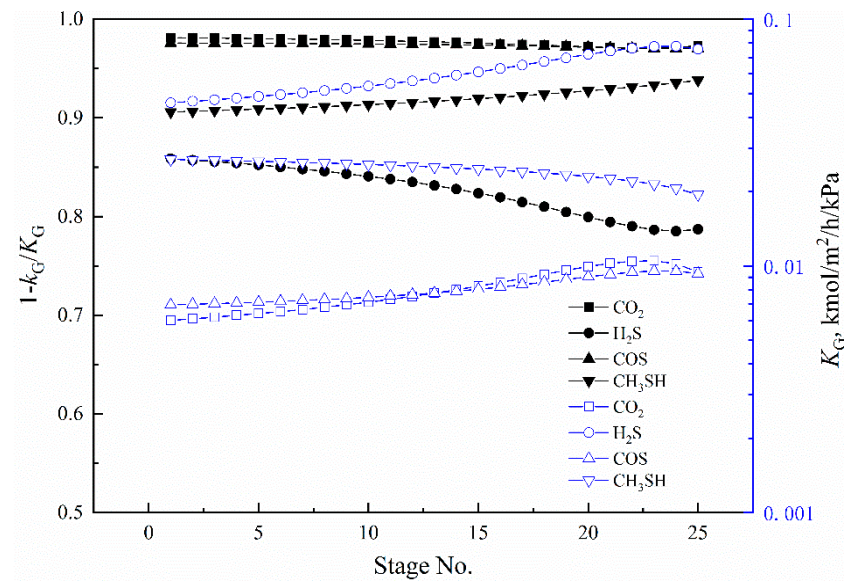


**Figure 11.** Total mass transfer coefficient and mass transfer resistance of different column positions (overflow weir height: 0.15 m; absorption pressure: 6 Mpa; inlet gas flow rate:  $5.0 \times 10^6 \text{ Nm}^3/\text{d}$ ; inlet gas–liquid ratio: 600; inlet gas loading:  $\text{CO}_2$ , 4.5 vol.%;  $\text{H}_2\text{S}$ , 1.5 vol.%; COS, 15  $\text{mg}/\text{m}^3$ ;  $\text{CH}_3\text{SH}$ , 15  $\text{mg}/\text{m}^3$ ).

For  $\text{CO}_2$  and COS, the gas mass transfer resistance can almost be ignored. In the whole absorption column, the gas mass transfer coefficient is less than  $0.01 \text{ kmol}/\text{m}^2/\text{kPa}$ . For  $\text{H}_2\text{S}$ , however, the gas mass transfer coefficient is almost ten times greater than that of  $\text{CO}_2$  and COS. Additionally, the liquid mass transfer coefficient of  $\text{H}_2\text{S}$  is also much higher than that of  $\text{CO}_2$  and COS, accounting for 15–25% of the total mass transfer resistance, so the gas-side mass transfer resistance cannot be ignored. The gas-side mass transfer resistance of  $\text{CH}_3\text{SH}$  accounts for 5–10% of the total mass transfer resistance, which also needs to be considered in the calculation process. This is consistent with the calculation method of the absorption model.

Based on the mass transfer characteristics analysis, the rate-limiting steps of absorption processes for different components can be clarified. Furthermore, it is helpful to simplify the model calculation.

#### 3.4. The Influence of the Operating Parameters

Based on the validated thermodynamic-absorption coupled model, the effects of gas-liquid ratio, overflow weir height, and absorption column pressure on the removal efficiency of each component were studied, and the results are shown in Figures 12–14. In addition, the effect of the acid component content in the feed gas on the removal efficiency of methyl mercaptan was studied, and the results are shown in Figure 15.

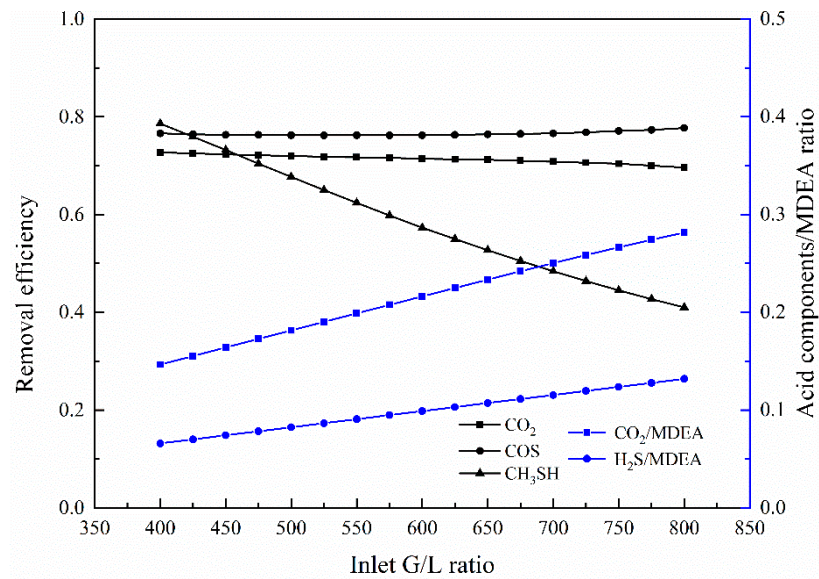


**Figure 12.** The effect of gas–liquid ratio on the removal efficiency and the acid components (CO<sub>2</sub> and H<sub>2</sub>S)/MDEA ratio (number of plates: 25; overflow weir height: 0.15 m; absorption pressure: 6 Mpa; inlet gas flow rate:  $5.0 \times 10^6$  Nm<sup>3</sup>/d; inlet gas loading: CO<sub>2</sub>, 4.5 vol.%; H<sub>2</sub>S, 1.5 vol.%; COS, 15 mg/m<sup>3</sup>; CH<sub>3</sub>SH, 15 mg/m<sup>3</sup>).

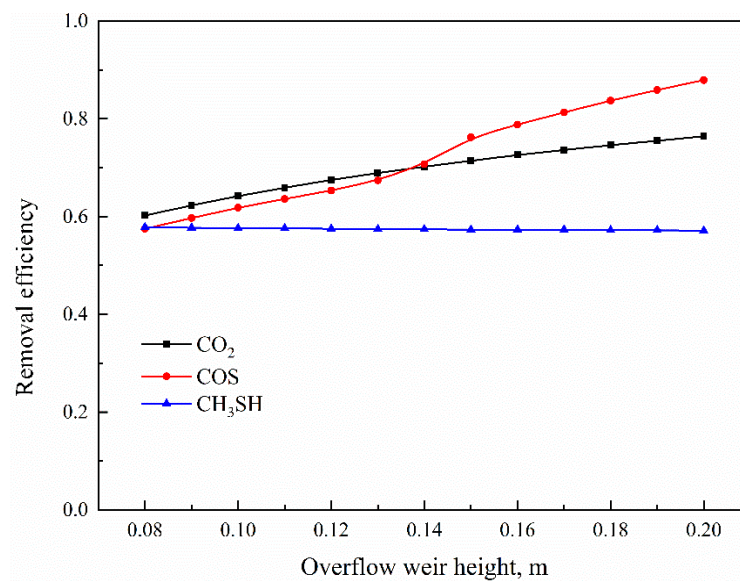


**Figure 13.** The effect of overflow weir height on removal efficiency (number of plates: 25; absorption pressure: 6 Mpa; inlet gas flow rate:  $5.0 \times 10^6$  Nm<sup>3</sup>/d; inlet gas–liquid ratio: 600; inlet gas loading: CO<sub>2</sub>, 4.5 vol.%; H<sub>2</sub>S, 1.5 vol.%; COS, 15 mg/m<sup>3</sup>; CH<sub>3</sub>SH, 15 mg/m<sup>3</sup>).

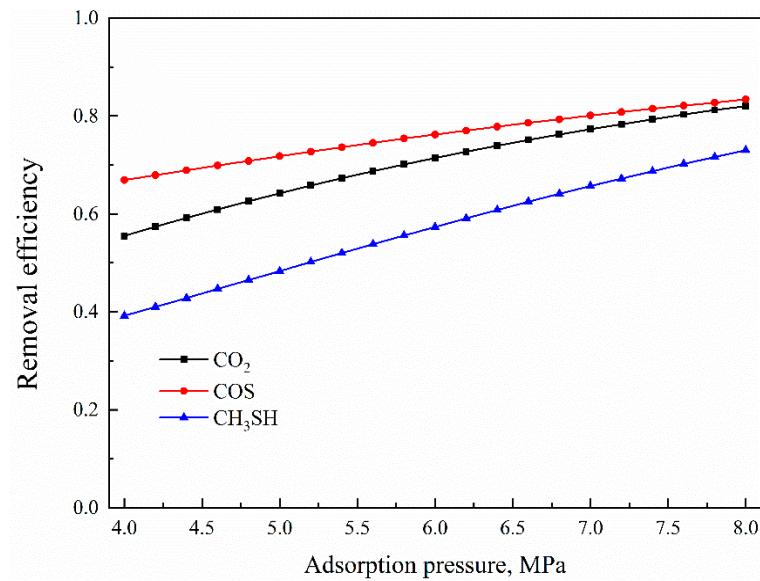


**Figure 14.** The effect of absorption pressure on removal efficiency (number of plates: 25; overflow weir height: 0.15 m; inlet gas flow rate:  $5.0 \times 10^6 \text{ Nm}^3/\text{d}$ ; inlet gas–liquid ratio: 600; inlet gas loading: CO<sub>2</sub>, 4.5 vol.%; H<sub>2</sub>S, 1.5 vol.%; COS, 15 mg/m<sup>3</sup>; CH<sub>3</sub>SH, 15 mg/m<sup>3</sup>).

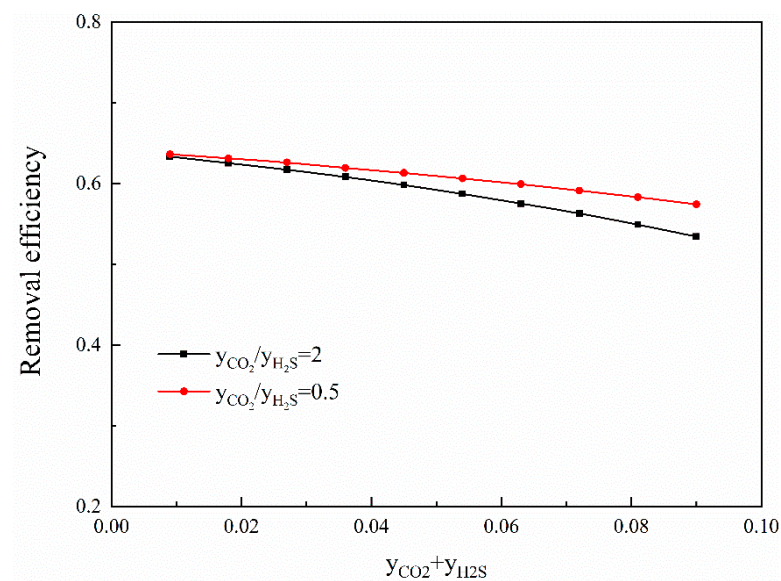


**Figure 15.** The effect of acid component content in feed gas on the removal efficiency of CH<sub>3</sub>SH (number of plates: 25; overflow weir height: 0.15 m; absorption pressure: 6 Mpa; inlet gas flow rate:  $5.0 \times 10^6 \text{ Nm}^3/\text{d}$ ; and inlet gas–liquid ratio: 600).

It can be seen from Figure 12 that the gas–liquid ratio has a greater impact on the absorption of CH<sub>3</sub>SH because CH<sub>3</sub>SH is physically absorbed and controlled by equilibrium. When the gas–liquid ratio increases from 400 to 800, the removal efficiency of CH<sub>3</sub>SH decreases from 0.8 to 0.4. Obviously, a more liquid phase is conducive to the physical absorption process. Since the absorption rate of CO<sub>2</sub> and COS is determined by mass transfer rate, it is less affected by the gas–liquid ratio.

Figure 13 shows the effect of the overflow weir height on the absorption performance of each component. As the reaction rate of CO<sub>2</sub> in the absorption solvent is very fast, the absorption rate is mainly controlled by the mass transfer rate of CO<sub>2</sub>. As the overflow weir height increases, the liquid thickness over the tray increases, and, thus, the mass transfer area increases, resulting in an increase in the removal rates of CO<sub>2</sub> and COS. For

CH<sub>3</sub>SH, the overflow weir height has little effect on its removal rate. One reason is that the absorption rate of CH<sub>3</sub>SH is controlled by its physical solubility in the mixed solvent. The second reason is that the increase in the overflow weir height strengthens the absorption of CO<sub>2</sub> and H<sub>2</sub>S, which reduces the solubility of CH<sub>3</sub>SH in the liquid phase. Figure 15 shows the effect of acid component content in the feed gas on the removal rate of CH<sub>3</sub>SH. As the acid component content increases, the absorption rate of CH<sub>3</sub>SH decreases significantly. The reason for this is that, as the acid component content in the liquid phase increases, the Henry constant of CH<sub>3</sub>SH absorption increases significantly.

The influence of tower pressure is shown in Figure 14. As the absorption pressure increases, the absorption driving force increases, and the removal efficiency of each component increases. Additionally, the physical absorption process is more sensitive to the tower pressure. With the increase in tower pressure, the removal efficiency of CH<sub>3</sub>SH achieves a significant increase when compared with the removal efficiency of CO<sub>2</sub> and COS. Due to the chemical absorption being the rate-limited step for the removal of CO<sub>2</sub> and COS, the absorption pressure on their removal efficiency is insignificant. As shown in Figure 14, the removal efficiency of COS increases by less than 10% when the absorption pressure increases from 4 MPa to 8 MPa.

#### 4. Conclusions

In this study, a rate-based absorption model coupled with a thermodynamic model was developed to characterize the removal of acid components (CO<sub>2</sub> and H<sub>2</sub>S) and organic sulfur (COS and CH<sub>3</sub>SH) from natural gas with an aqueous sulfolane–MDEA solution. The thermodynamic model was improved by improving the calculation method of the chemical equilibrium constant and by incorporating the influence of acid components for COS removal, which made the gas–liquid equilibrium (GLE) data more accurate. The absorption model was validated by the experimental data obtained from an industrial device, and the average relative errors of the removal rates of CO<sub>2</sub>, COS, and CH<sub>3</sub>SH obtained by experiment and calculation are 3.3%, 3.0%, and 4.1%, respectively. The validated coupled model indicated that the gas mass transfer resistance can almost be ignored for CO<sub>2</sub> and COS, but both gas and liquid mass transfer resistance for H<sub>2</sub>S and CH<sub>3</sub>SH should be considered. Additionally, the analysis of influencing factors shows that the gas–liquid ratio has a greater impact on the physical absorption process controlled by equilibrium but has a limited effect on the absorption process determined by a chemical reaction. An increased overflow weir height increases the gas–liquid contact time and mass transfer area, thus resulting in an increase in the removal rates of CO<sub>2</sub> and COS, which, however, inhibits the absorption of CH<sub>3</sub>SH due to the increased Henry coefficient. Furthermore, the physical absorption process rather than the chemical absorption process is more sensitive to the tower pressure.

**Author Contributions:** Conceptualization, K.L. and J.L.; Formal analysis, K.L., G.X., J.H. and Q.L.; Funding acquisition, J.L.; Investigation, K.L.; Methodology, K.L.; Resources, J.L.; Software, H.C.; Writing—original draft, K.L.; Writing—review & editing, K.L. and J.L. All authors have read and agreed to the published version of the manuscript.

**Funding:** This research received no external funding.

**Institutional Review Board Statement:** Not applicable.

**Informed Consent Statement:** Not applicable.

**Data Availability Statement:** Not applicable.

**Conflicts of Interest:** The authors declare no conflict of interest.

## Nomenclature

$P$	system pressure	Pa
$y_i$	mole fraction of component $i$ in the vapor phase	-
$x_i$	mole fraction of component $i$ in the liquid phase	-
$H_i$	Henry's law constant of component $i$	Pa m <sup>3</sup> /mol
$\varphi_i$	fugacity coefficient of component $i$ in the vapor phase	-
$\gamma_i^*$	unsymmetric activity coefficient in the mixed solvent solution	-
$w_A$	weighting factor	-
$\gamma^\infty$	infinite dilution activity coefficient	-
$H_{iA}$	Henry's constant of component $i$ in pure solvent A	Pa m <sup>3</sup> /mol
$H_{CH_3SH}$	Henry's constants of CH <sub>3</sub> SH considering the influence of acid gas	Pa m <sup>3</sup> /mol
$H_{CH_3SH}'$	Henry's constants of CH <sub>3</sub> SH ignoring the influence of acid gas	Pa m <sup>3</sup> /mol
$f$	unremoved rate of MDEA	
$c$	effect factor	
$K$	chemical equilibrium constant	
$F$	mole flow rate of feed	kmol/s
$L$	mole flow rate of liquid	kmol/s
$V$	mole flow rate of vapor	kmol/s
$N$	mole transfer rate	kmol/s
$Q$	heat input	J/s
$q$	heat transfer rate	J/s
$H^F$	enthalpy of feed	J/kmol
$H^V$	enthalpy of the vapor	J/kmol
$H^L$	enthalpy of the liquid	J/kmol
$K_G$	overall mass transfer coefficient	kmol/m <sup>2</sup> s kPa
$P_i^*$	partial pressure of component $i$ in equilibrium with the liquid phase	-
$P_i$	partial pressure of component $i$ in the gas bulk	-
$a_p$	effective mass transfer area of the column per unit area of the tray	m <sup>2</sup> /m <sup>2</sup>
$A_c$	cross-sectional area of the column	m <sup>2</sup>
$k_G$	mass transfer coefficient without reaction in the gas phase	kmol/m <sup>2</sup> s kPa
$k_L$	mass transfer coefficient without reaction in the liquid phase	m/s
$E$	enhancement factor	-
$Ha$	Hatta number	-
$E_\infty$	enhancement number for infinite fast reactions	-
$D_L$	diffusivity in an aqueous sulfolane–MDEA solution	m <sup>2</sup> /s
$C^{In}$	concentration at the gas–liquid interface	kmol/m <sup>3</sup>
$C^{Bulk}$	concentration in the bulk liquid	kmol/m <sup>3</sup>
$k_{2t}$	rate constant	m <sup>3</sup> /kmol s
$T$	temperature	K
Subscripts		
$i$	component $i$	
$i'$	product $i'$	
$j$	stage number	
Superscripts		
$L$	liquid phase	
$V$	vapor phase	

## References

1. Bolh ar-Nordenkampf, M.; Friedl, A.; Koss, U.; Tork, T. Modelling selective H<sub>2</sub>S absorption and desorption in an aqueous MDEA-solution using a rate-based non-equilibrium approach. *Chem. Eng. Process.* **2004**, *43*, 701–715. [[CrossRef](#)]
2. Baccanelli, M.; Lang e, S.; Rocco, M.V.; Pellegrini, L.A.; Colombo, E. Low temperature techniques for natural gas purification and LNG production: An energy and exergy analysis. *Appl. Energy* **2016**, *180*, 546–559. [[CrossRef](#)]
3. Song, C.; Liu, Q.; Ji, N.; Deng, S.; Zhao, J.; Kitamura, Y. Natural gas purification by heat pump assisted MEA absorption process. *Appl. Energy* **2017**, *204*, 353–361. [[CrossRef](#)]

4. Shirazizadeh, H.A.; Haghtalab, A. Simultaneous solubility measurement of (ethyl mercaptan plus carbon dioxide) into the aqueous solutions of (N-methyl diethanolamine plus sulfolane plus water). *J. Chem. Thermodyn.* **2019**, *133*, 111–122. [[CrossRef](#)]
5. Amararene, F.; Bouallou, C. Kinetics of carbonyl sulfide (COS) absorption with aqueous solutions of diethanolamine and methyldiethanolamine. *Ind. Eng. Chem. Res.* **2004**, *43*, 6136–6141. [[CrossRef](#)]
6. Huttenhuis, P.J.G.; Agrawal, N.J.; Versteeg, G.F. Solubility of carbon dioxide and hydrogen sulfide in aqueous N-methyldiethanolamine solutions. *Ind. Eng. Chem. Res.* **2009**, *48*, 4051–4059. [[CrossRef](#)]
7. Gutierrez, J.P.; Benitez, L.A.; Ale Ruiz, E.L.; Erdmann, E. A sensitivity analysis and a comparison of two simulators performance for the process of natural gas sweetening. *J. Nat. Gas Sci. Eng.* **2016**, *31*, 800–807. [[CrossRef](#)]
8. Xu, S.; Wang, Y.W.; Otto, F.D.; Mather, A.E. The physicochemical properties of the mixed-solvent of 2-piperidineethanol, sulfolane and water. *J. Chem. Technol. Biotechnol.* **1993**, *56*, 309–316. [[CrossRef](#)]
9. Amararene, F.; Bouallou, C. Study of hydrogen sulfide absorption with diethanolamine in methanolic aqueous solutions. *Chem. Eng. Trans.* **2016**, *52*, 259–264.
10. Zhang, Y.; Chen, C.-C. Thermodynamic modeling for CO<sub>2</sub> absorption in aqueous MDEA solution with electrolyte NRTL model. *Ind. Eng. Chem. Res.* **2011**, *50*, 163–175. [[CrossRef](#)]
11. Zhang, Y.; Chen, C.-C. Modeling Gas Solubilities in the Aqueous Solution of Methyldiethanolamine. *Ind. Eng. Chem. Res.* **2011**, *50*, 6436–6446. [[CrossRef](#)]
12. Austgen, D.M.; Rochelle, G.T.; Peng, X.; Chen, C.C. Model of vapor-liquid equilibria for aqueous acid gas-alkanolamine systems using the electrolyte-NRTL equation. *Ind. Eng. Chem. Res.* **1989**, *28*, 1060–1073. [[CrossRef](#)]
13. Zong, L.; Chen, C.-C. Thermodynamic modeling of CO<sub>2</sub> and H<sub>2</sub>S solubilities in aqueous DIPA solution, aqueous sulfolane-DIPA solution, and aqueous sulfolane–MDEA solution with electrolyte NRTL model. *Fluid Phase Equilibria* **2011**, *306*, 190–203. [[CrossRef](#)]
14. Macgregor, R.J.; Mather, A.E. Equilibrium solubility of H<sub>2</sub>S and CO<sub>2</sub> and their mixtures in a mixed solvent. *Can. J. Chem. Eng.* **1991**, *69*, 1357–1366. [[CrossRef](#)]
15. Jou, F.Y.; Mather, A.E.; Ng, H.J. Effect of CO<sub>2</sub> and H<sub>2</sub>S on the solubility of methanethiol in an aqueous methyldiethanolamine solution. *Fluid Phase Equilibria* **1999**, *158–160*, 933–938. [[CrossRef](#)]
16. Haghtalab, A.; Eghbali, H.; Shojaeian, A. Experiment and modeling solubility of CO<sub>2</sub> in aqueous solutions of diisopropanolamine+2-amino-2-methyl-1-propanol+Piperazine at high pressures. *J. Chem. Thermodyn.* **2014**, *71*, 71–83. [[CrossRef](#)]
17. Kaur, H.; Chen, C.-C. Thermodynamic modeling of CO<sub>2</sub> absorption in aqueous potassium carbonate solution with electrolyte NRTL model. *Fluid Phase Equilibria* **2020**, *505*, 112339–112350. [[CrossRef](#)]
18. Simon, L.L.; Elias, Y.; Puxty, G.; Artanto, Y.; Hungerbuhler, K. Rate based modeling and validation of a carbon-dioxide pilot plant absorption column operating on monoethanolamine. *Chem. Eng. Res. Des.* **2011**, *89*, 1684–1692. [[CrossRef](#)]
19. Borhani, T.N.G.; Afkhamipour, M.; Azarpour, A.; Akbari, V.; Emadi, S.H.; Manan, Z.A. Modeling study on CO<sub>2</sub> and H<sub>2</sub>S simultaneous removal using MDEA solution. *J. Ind. Eng. Chem.* **2016**, *34*, 344–355. [[CrossRef](#)]
20. Zhang, Y.; Chen, H.; Chen, C.-C.; Plaza, J.M.; Dugas, R.; Rochelle, G.T. Rate-based process modeling study of CO<sub>2</sub> capture with aqueous monoethanolamine solution. *Ind. Eng. Chem. Res.* **2009**, *48*, 9233–9246. [[CrossRef](#)]
21. Afkhamipour, M.; Mofarahi, M. Comparison of rate-based and equilibrium-stage models of a packed column for post-combustion CO<sub>2</sub> capture using 2-amino-2-methyl-1-propanol (AMP) solution. *Int. J. Greenh. Gas Control* **2013**, *15*, 186–199. [[CrossRef](#)]
22. Al-Baghli, N.A.; Pruess, S.A.; Yesavage, V.F.; Selim, M.S. A rate-based model for the design of gas absorbers for the removal of CO<sub>2</sub> and H<sub>2</sub>S using aqueous solutions of MEA and DEA. *Fluid Phase Equilibria* **2001**, *185*, 31–43. [[CrossRef](#)]
23. Pacheco, M.A.; Rochelle, G.T. Rate-based modeling of reactive absorption of CO<sub>2</sub> and H<sub>2</sub>S into aqueous methyldiethanolamine. *Ind. Eng. Chem. Res.* **1998**, *37*, 4107–4117. [[CrossRef](#)]
24. Mandal, B.; Bandyopadhyay, S.S. Simultaneous absorption of CO<sub>2</sub> and H<sub>2</sub>S into aqueous blends of N-methyldiethanolamine and diethanolamine. *Environ. Sci. Technol.* **2006**, *40*, 6076–6084. [[CrossRef](#)]
25. Moioli, S.; Pellegrini, L.A.; Picutti, B.; Vergani, P. Improved rate-based modeling of H<sub>2</sub>S and CO<sub>2</sub> removal by methyldiethanolamine scrubbing. *Ind. Eng. Chem. Res.* **2013**, *52*, 2056–2065. [[CrossRef](#)]
26. Yang, C.; Liu, K.; Li, L.; Wang, J.; Hu, T.; Zhang, X. Research on the factors affecting organic sulfur removal of natural gas purification unit. *Chem. Eng. Oil Gas* **2021**, *50*, 9–16.
27. Peng, D.-Y.; Robinson, D.B. A New two-constant equation of state. *Ind. Eng. Chem. Fundam.* **1976**, *15*, 59–64. [[CrossRef](#)]
28. Van Ness, H.C.; Abbott, M.M. Vapor-liquid equilibrium. Part VI. standard state fugacities for supercritical components. *AIChE J.* **1979**, *25*, 645–653. [[CrossRef](#)]
29. Bedell, S.A.; Miller, M. Aqueous amines as reactive solvents for mercaptan removal. *Ind. Eng. Chem. Res.* **2007**, *46*, 3729–3733. [[CrossRef](#)]
30. Shokouhi, M.; Farahani, H.; Vahidi, M.; Taheri, S.A. Experimental solubility of carbonyl sulfide in sulfolane and  $\gamma$ -butyrolactone. *J. Chem. Eng. Data* **2017**, *62*, 3401–3408. [[CrossRef](#)]
31. Jou, F.Y.; Deshmukh, R.D.; Otto, F.D.; Mather, A.E. Solubility of H<sub>2</sub>S, CO<sub>2</sub>, CH<sub>4</sub> and C<sub>2</sub>H<sub>6</sub> in sulfolane at elevated pressures. *Fluid Phase Equilibria* **1990**, *56*, 313–324. [[CrossRef](#)]
32. Al-Ghawas, H.A.; Ruiz-Ibanez, G.; Sandall, O.C. Absorption of carbonyl sulfide in aqueous methyldiethanolamine. *Chem. Eng. Sci.* **1989**, *44*, 631–639. [[CrossRef](#)]

33. Song, Y.H.; Chen, C.C. Symmetric electrolyte nonrandom two-liquid activity coefficient model. *Ind. Eng. Chem. Res.* **2009**, *48*, 7788–7797. [[CrossRef](#)]
34. Chen, C.-C.; Britt, H.I.; Boston, J.F.; Evans, L.B. Local composition model for excess Gibbs energy of electrolyte systems. Part I: Single solvent, single completely dissociated electrolyte systems. *AIChE J.* **1982**, *28*, 588–596. [[CrossRef](#)]
35. Cleeton, C.; Kvam, O.; Rea, R.; Sarkisov, L.; De Angelis, M.G. Competitive H<sub>2</sub>S-CO<sub>2</sub> absorption in reactive aqueous methyldiethanolamine solution: Prediction with ePC-SAFT. *Fluid Phase Equilibria* **2020**, *511*, 112453–112468. [[CrossRef](#)]
36. Austgen, D.M.; Rochelle, G.T.; Chen, C.C. Model of vapor-liquid equilibria for aqueous acid gas-alkanolamine systems. 2. Representation of hydrogen sulfide and carbon dioxide solubility in aqueous MDEA and carbon dioxide solubility in aqueous mixtures of MDEA with MEA or DEA. *Ind. Eng. Chem. Res.* **1991**, *30*, 543–555. [[CrossRef](#)]
37. Hairul, N.A.H.; Shariff, A.M.; Tay, W.H.; Mortel, A.M.A.V.D.; Lau, K.K.; Tan, L.S. Modelling of high pressure CO<sub>2</sub> absorption using PZ plus AMP blended solution in a packed absorption column. *Sep. Purif. Technol.* **2016**, *165*, 179–189. [[CrossRef](#)]
38. Almoslh, A.; Alobaid, F.; Heinze, C.; Epple, B. Comparison of equilibrium-stage and rate-based models of a packed column for tar absorption using vegetable oil. *Appl. Sci.* **2020**, *10*, 2362. [[CrossRef](#)]
39. Treybal, R.E. Adiabatic gas absorption and stripping in packed towers. *Ind. Eng. Chem.* **1969**, *61*, 36–41. [[CrossRef](#)]
40. Saimpert, M.; Puxty, G.; Qureshi, S.; Wardhaugh, L.; Cousins, A. A new rate based absorber and desorber modelling tool. *Chem. Eng. Sci.* **2013**, *96*, 10–25. [[CrossRef](#)]
41. Danckwerts, P.V. Absorption by simultaneous diffusion and chemical reaction. *Trans. Faraday Soc.* **1950**, *46*, 300–304. [[CrossRef](#)]
42. DeCoursey, W.J. Enhancement factors for gas absorption with reversible reaction. *Chem. Eng. Sci.* **1982**, *37*, 1483–1489. [[CrossRef](#)]
43. Jou, F.-Y.; Carroll, J.J.; Mather, A.E.; Otto, F.D. The solubility of carbon dioxide and hydrogen sulfide in a 35 wt% aqueous solution of methyldiethanolamine. *Can. J. Chem. Eng.* **1993**, *71*, 264–268. [[CrossRef](#)]
44. Qian, W.-M.; Li, Y.-G.; Mather, A.E. Correlation and prediction of the solubility of CO<sub>2</sub> and H<sub>2</sub>S in an aqueous solution of methyldiethanolamine and sulfolane. *Ind. Eng. Chem. Res.* **1995**, *34*, 2545–2550. [[CrossRef](#)]
45. Sidi-Boumedine, R.; Horstmann, S.; Fischer, K.; Provost, E.; Fürst, W.; Gmehling, J. Experimental determination of hydrogen sulfide solubility data in aqueous alkanolamine solutions. *Fluid Phase Equilibria* **2004**, *218*, 149–155. [[CrossRef](#)]